Computational and Structural Biotechnology Journal 23 (2024) 1477–1488

Contents lists available at ScienceDirect

Computational and Structural Biotechnology Journal

journal homepage: www.elsevier.com/locate/csbj

Research article

Structure-guided identification and characterization of potent inhibitors targeting PhoP and MtrA to combat mycobacteria

Han-Li Su [a,1], Shu-Jung Lai [b,c,1], Keng-Chang Tsai [d,e,1], Kit-Man Fung [f], Tse-Lin Lung [g], Hsing-Mien Hsu [g], Yi-Chen Wu [g], Ching-Hui Liu [g], Hui-Xiang Lai [g], Jiun-Han Lin [h,i], Tien-Sheng Tseng [g,*]

[a] Department of Emergency Medicine, Ditmanson Medical Foundation Chia-Yi Christian Hospital, Chiayi City 600, Taiwan
[b] Graduate Institute of Biomedical Sciences, China Medical University, Taichung, Taiwan
[c] Research Center for Cancer Biology, China Medical University, Taichung, Taiwan
[d] National Research Institute of Chinese Medicine, Ministry of Health and Welfare, Taipei, Taiwan
[e] Ph.D. Program in Medical Biotechnology, College of Medical Science and Technology, Taipei Medical University, Taipei, Taiwan
[f] Biomedical Translation Research Center (BioTReC), Academia Sinica, Taipei 11529, Taiwan
[g] Institute of Molecular Biology, National Chung Hsing University, Taichung,Taiwan
[h] Department of Industrial Technology, Ministry of Economic Affairs, Taipei, Taiwan
[i] Food Industry Research and Development Institute, Hsinchu City, Taiwan

ARTICLE INFO

Keywords:
Tuberculosis
Drug-resistant tuberculosis
Two-component signal transduction systems
Pharmacophore-based inhibitor screening
Mycobacteria

ABSTRACT

Mycobacteria are causative agents of tuberculosis (TB), which is a global health concern. Drug-resistant TB strains are rapidly emerging, thereby necessitating the urgent development of new drugs. Two-component signal transduction systems (TCSs) are signaling pathways involved in the regulation of various bacterial behaviors and responses to environmental stimuli. Applying specific inhibitors of TCSs can disrupt bacterial signaling, growth, and virulence, and can help combat drug-resistant TB. We conducted a comprehensive pharmacophore-based inhibitor screening and biochemical and biophysical examinations to identify, characterize, and validate potential inhibitors targeting the response regulators PhoP and MtrA of mycobacteria. The constructed pharmacophore model Phar-PR-n4 identified effective inhibitors of formation of the PhoP–DNA complex: ST132 (IC_{50} = 29 ± 1.6 μM) and ST166 (IC_{50} = 18 ± 1.3 μM). ST166 (KD = 18.4 ± 4.3 μM) and ST132 (KD = 14.5 ± 0.1 μM) strongly targeted PhoP in a slow-on, slow-off manner. The inhibitory potency and binding affinity of ST166 and ST132 for MtrAC were comparable to those of PhoP. Structural analyses and molecular dynamics simulations revealed that ST166 and ST132 mainly interact with the α8-helix and C-terminal β-hairpin of PhoP, with functionally essential residue hotspots for structure-based inhibitor optimization. Moreover, ST166 has in vitro antibacterial activity against *Macrobacterium marinum*. Thus, ST166, with its characteristic 1,2,5,6-tetrathiocane and terminal sulphonic groups, has excellent potential as a candidate for the development of novel antimicrobial agents to combat pathogenic mycobacteria.

1. Introduction

Mycobacterium tuberculosis (*Mtb*) is the causative agent of tuberculosis (TB)[1]. Tuberculosis (TB) is a persistent health problem that ranks as the 13th leading cause of death worldwide [2]; since 2012, it has been the leading cause of death among infectious diseases. Despite numerous efforts, the control of TB remains challenging. In 2021, TB is estimated to affect approximately 10.6 million people worldwide[3]. The World

Abbreviations: CADD, Computer-aided drug design; CADDD, Computer-aided drug discovery and development; CTD, C-terminal domain; DBD, DNA-binding domain; FP, Fluorescence polarization; HK, Histidine kinase; LB, Luria-Bertani, LBDD, Ligand-based drug design; LSPR, Localized surface plasmon resonance; MD, Molecular dynamics, MDR, Multi-drug-resistant; MIC, Minimum inhibitory concentration; PME, Particle Mesh Ewald; RMSD, Root mean square deviation; RMSF, Root mean square fluctuation; RR, Response regulator; SBDD, Structure-based drug design; TCS, Transduction system.

* Corresponding author.
E-mail addresses: i90221141ster@gmail.com, emersontseng@dragon.nchu.edu.tw (T.-S. Tseng).
[1] Equal contribution

https://doi.org/10.1016/j.csbj.2024.04.005
Received 24 December 2023; Received in revised form 1 April 2024; Accepted 1 April 2024
Available online 3 April 2024

Health Organization reported that the greatest share of the global TB burden fell in Southeast Asia (45% of all cases), followed by Africa (23%). Therefore, targeted interventions are necessary to effectively combat this disease. However, the emergence of multi-drug-resistant (MDR), extensively drug-resistant (XDR), and rifampicin-resistant TB has hindered efforts to effectively create an epidemic within the broader TB problem. Estimates indicate that, 450,000–470,000 cases of MDR/XDR-TB in in 2021 resulted in 191,000 fatalities[4]. Novel drugs must be developed to combat the threat to global public health caused by the rapid emergence of MDR- and XDR-TB.

The survival and persistence of bacteria within a host organism depends on their ability to sense and adapt to their environment[5–9]. One crucial mechanism involved in this process is the two-component signal transduction system (TCS)[10–13]. A typical TCS has two main components: histidine kinase (HK) and response regulator (RR)[10–13]. HK is a sensor that detects environmental signals such as temperature, pH, nutrient availability, and the presence of antimicrobial compounds. HKs are transmembrane proteins comprising a periplasmic N-terminal sensing domain and a cytoplasmic/catalytic C-terminal domain (CTD). The CTDs of HKs contain a dimerization domain and an ATP-binding kinase domain. On sensing a signal, HK undergoes autophosphorylation and transfers a phosphate group from ATP to a conserved histidine residue in its catalytic domain. The phosphoryl group is transferred from HK to the cognate RR, which typically contains a conserved aspartate residue in its receiver domain. RRs are mainly transcription factors comprising an N-terminal receiver domain and C-terminal DNA-binding domain (DBD). This phosphorylation event triggers a conformational change in the RR, which leads to its activation and subsequent regulation of downstream genes or cellular processes [14]. Hence, bacteria use TCSs to adjust their behavior, physiology, and gene expression patterns in response to specific signals encountered within their host or the external environment, thereby enabling them to evade host immune responses, establish persistent infections, form biofilms, acquire antibiotic resistance, and exhibit pathogenicity. Moreover, TCSs are found only in bacteria, and not in humans. Therefore, targeting the TCS components is a promising method for developing new antimicrobial agents that can disrupt bacterial adaptation, enhance host immune responses, and overcome antibiotic resistance [15–21].

Two key TCS RRs of *Mtb*, MtrA (Rv3246c) and PhoP (Rv0757), control drug resistance and virulence of *Mtb*. MrtA is one of 11 essential pairs of TCSs *Mtb* [22]. Phosphorylated MrtA binds to the promoters of *dnaA*, *fapB*, *oriA*, and *ripA* [23,24]. The MrtA/B system modulates lipoprotein activity in *Mtb* to regulate drug resistance and cell wall homeostasis[25]. MtrA is differentially expressed in avirulent and virulent strains during macrophage[22]. MtrA not only controls cell division [26] and cell wall metabolism, but also affects the susceptibility of *Mtb* to first-line anti-TB drugs[26]. Thus, MtrA is a key target for antimicrobial drugs[27,28]. Another TCS, PhoP/R, regulates the expression of more than 100 genes of *Mtb* [29]. Deletion of *phoP* or *phoR* genes can considerably attenuate the virulence of *Mtb* [30,31]. PhoP/Rs are also involved in the synthesis of complex cell wall lipids[30]. Thus, inhibitors of PhoP/R function could also be developed for use as anti-tuberculosis agents. Additionally, MtrA and PhoP have sequence and structural similarities in their C-terminal DBD[32], thereby suggesting that targeting this region could be broadly effective if the activities of multiple RRs are disrupted simultaneously. Inhibitors that specifically or simultaneously target the C-terminal DBDs of these RRs can disrupt their binding to DNA and prevent the subsequent regulation of gene expression.

Computer-aided drug design (CADD) is an efficient and cost-effective method for rapidly identifying inhibitors with specific biological activities such as those targeting the RRs of TCSs[33]. CADD methods include the structure-based drug design (SBDD) and ligand-based drug design (LBDD) methods. SBDD is more commonly used than LBDD because it relies on widely available crystallographic structures for various biological targets[34–36]. Conversely, LBDD requires structural information about the target, which may be limited[35,36]. SBDD methods can be further classified into pharmacophore modeling and molecular docking methods[37]. Molecular docking is a virtual high-throughput screening method used to evaluate the potential biological activities of compounds based on their structural properties[38]. In contrast, pharmacophore modeling can explore and define the arrangement of essential features of a ligand that enables it to specifically and effectively bind to a receptor[39,40]. The generation of receptor–ligand pharmacophores can reveal molecular features by converting protein properties into reciprocal ligand spaces. Hence, pharmacophore modeling enables the effective design of ligands with properties necessary for effective binding to a specific protein,[41] and numerous studies have reported that this method can accelerate the drug discovery process[42–46]. Thus, pharmacophore-based screening, known for its efficacy in identifying novel inhibitors that potentially exhibit biological activity[39,40,47,48,49], was employed in this study.

Protein structures have been identified for the *Mtb* RRs of the MtrA-apo [50]and PhoP–DNA complexes[51]. This structural information for MtrA-apo (PDB ID: 2GWR) and the PhoP–DNA complex (PDB ID: 5ED4) enabled the use of CADD to screen for and develop potent inhibitors. In this study, pharmacophore-based inhibitor screening was coupled with biochemical and biophysical examinations to identify, characterize, and validate potential inhibitors of the PhoP–DNA complex. Receptor–ligand-pharmacophore generation was used to comprehensively explore the functionally essential features of DNA–PhoP interactions. A pharmacophore model, Phar-PR-n4, was developed and employed to identify three out of 68,000 compounds from the IBS database that showed 50% inhibition against the formation of PhoP–DNA complex at a compound concentration of 100 μM. A further inhibition assay demonstrated that ST166 (IC_{50} = 18 ± 1.3 μM), ST132 (IC_{50} = 29 ± 1.6 μM), and ST950 (IC_{50} = 88 ± 1.2 μM) all exhibited dose-dependent inhibition that disrupted PhoP–DNA complex formation. Localized surface plasmon resonance (LSPR) investigations revealed that the binding affinities of ST166 and ST132 to PhoP are 18.4 ± 4.3 and 14.5 ± 0.1 μM, respectively. In addition, the inhibitory potency and binding affinity of ST166 and ST132 for MtrA were investigated and compared with those of PhoP. The modes of action of ST166 and ST132 on PhoP and MtrA were investigated using structural analysis and molecular dynamics (MD) simulations. Finally, the in vitro antibacterial activity of ST166 was characterized and confirmed for a *Mycobacterium* species (*Macrobacterium marinum*). This integrated approach of combining CADD with biochemical and biophysical techniques successfully identified, characterized, and validated an inhibitor, ST166, that specifically targets both PhoP and MtrA in *Mtb*. ST166 can be further optimized to develop therapeutic agents for combating pathogenic *Mycobacterium* species.

2. Materials and methods

2.1. Preparation of the recombinant MtrAC and PhoP proteins

An expression plasmid for full-length PhoP was designed by inserting the *phoP* gene into a pET28a vector (*Nde*I and *Xho*I restriction enzyme sites) with an N-terminal His-tag. The nucleotide sequence encoding the DBD of MtrA (MtrAC) was cloned into the pET28a vector at *Nde*I and *Xho*I restriction sites using an N-terminal His-tag. All genes were synthesized and subcloned into the expression vectors of interest by Yao-Hong Biotechnology, Inc. (https://www.yh-bio.info/). The PhoP plasmid was transformed into *Escherichia coli* (Shuffle T7). Bacteria were cultured in Luria-Bertani (LB) medium at 37 °C with 50 mg/L kanamycin. When the cell density reached OD_{600} = 0.6, the culture was treated with 0.05 mM IPTG for induction and was incubated at 30 °C overnight. The MtrAC plasmid was transformed into *E. coli* [BL21 (DE3)] and cultured in LB medium at 37 °C with 50 mg/L kanamycin. The culture was then induced (0.2 mM IPTG for 4 h at 37 °C) at an OD_{600} of 0.6. All cultured cells were harvested by centrifugation (6000 rpm for

20 min), resuspended in lysis buffer (20 mM Tris-HCl and 100 mM NaCl at pH 8.0), and disrupted using a microfluidizer (Microfluidics). The supernatant of the resulting crude extract was purified using nickel–nitrilotriacetic acid affinity resins (Qiagen, Hilden, Germany) and further purified using size-exclusion chromatography (Superdex 75 Increase 10/300 GL). The purity of the samples was verified using a Coomassie blue-stained SDS polyacrylamide gel.

2.2. Preparations of DNA fragments

The double-stranded oligonucleotides 5′-GGCGGTGTAGTTATCACGCCGTTT-3′ (fragment of *dna A* promoter region) and 3′-ATCTACGACACTTAGTCGACACTTAG-5′ used for biophysical studies of MtrA [52] and PhoP[51], respectively, were synthesized by and purchased from Yao-Hong Biotechnology. Double-stranded DNA was annealed by mixing equal aliquots of the two oligomers in 20 mM sodium phosphate buffer and 50 mM NaCl (pH 7.0), heating the mixture to 95 °C, and then slowly cooling it to room temperature. Subsequently, ion exchange chromatography [Mono-Q 5/50 GL column; Amersham Biosciences)] was used to purify the annealed double-stranded DNA.

Analyses of DNA-binding properties of MtrA and PhoP through fluorescence polarization assay.

The oligonucleotides used for the fluorescence polarization (FP) experiment (5′-GGCGGTGTAGTTATCACGCCGTTT-3′ and 3′-ATCTACGACACTTAGTCGACACTTAG-5′) were labeled with 6-carboxyfluorescein (6-FAM) at the 5′ positions. The proteins PhoP and MtrAC were added at appropriate concentrations to wells containing 10 nM 6-FAM-labeled DNA in reaction buffer (20 mM sodium phosphate and 50 mM NaCl at pH 7.0) at 25 °C. A Synergy H1MF plate reader (BioTek Instruments, Inc.) was used to measure the reactions thrice at excitation and emission wavelengths of 485 and 535 nm, respectively. The binding curves were fitted to one or two binding models. Data were analyzed and plotted using the Prism software (version 6; GraphPad, San Diego, CA, USA).

Receptor–ligand-pharmacophore generation and pharmacophore-based inhibitor screening (ligand-pharmacophore mapping).

Receptor–ligand-pharmacophore modeling can precisely identify the functionally critical features of ligands that interact with target proteins. Thus, we used the PhoP–DNA complex structure (PDB ID: 5ED4) to construct a pharmacophore model of these interactive features for screening inhibitors. The receptor–ligand-pharmacophore generation module in Discovery Studio 2021 (Accelrys Software, San Diego, CA, USA) was used to generate a pharmacophore model. The PhoP structure served as the input receptor and the DNA structure was used as the input ligand. The minimum and maximum feature values were 10 and 30, respectively, whereas the maximum pharmacophore value was 10. Conformation generation was performed with the “fast” and “rigid fitting” settings. The remaining parameters were set to default values. The constructed pharmacophore model was then used for ligand-pharmacophore mapping by fitting all molecules in the IBS database (https://www.ibscreen.com/; 68,000 compounds). The fitting method was set to “flexible,” and all other parameters were the defaults.

2.3. Inhibitory activities of compounds as determined through FP measurements

The oligonucleotide (3′-ATCTACGACACTTAGTCGACACTTAG-5′) retrieved from the determined PhoP–DNA complex [51] and labeled with 6-FAM at the 5′ position was dissolved in 20 mM sodium phosphate and 50 mM NaCl at pH 7.0 for FP experiments. Approximately 10 μl of PhoP (prepared in 20 mM sodium phosphate and 50 mM NaCl at pH 7.0) was first added to the wells of an ELISA plate. Next, 1 μl of serially diluted inhibitors (prepared in the same buffer as PhoP) was mixed with PhoP (final concentration 20 μM) to reach the desired concentrations, and the plate was incubated at 25 °C for 10 min. Subsequently, 9 μl of 6-FAM-labeled DNA (final concentration = 10 nM) was added, followed by incubation at 25 °C for another 10 min. The reactions were measured three times using a Synergy H1MF plate reader (BioTek Instruments, Inc.) at excitation and emission wavelengths of 485 and 535 nm, respectively. The percentage inhibition was calculated using the following equation:

$$Inhibition\% = \frac{\{[(P+D)-(D)]-[(P+I+D)-(D)]\}}{[(P+D)-(D)]} \times 100$$

where (D), $(P+D)$, and $(P+I+D)$ represent the polarization intensities of DNA alone, PhoP bound to DNA, and PhoP mixed with the inhibitor and then incubated with DNA, respectively. The MtrAC inhibitory activities of the identified compounds were also determined with this method but using the other oligonucleotide (3′-ATCTACGACACTTAGTCGACACTTAG-5′) with the 5′ end 6-FAM labeled.

LSPR.

The protein-binding affinities of the identified inhibitors were determined and analyzed using an OpenSPR instrument (Nicoya Life Science, Inc.). The protein solution was prepared in 1 × PBS at pH 7.3. The protein (80 μg/ml) was immobilized on a Ni^{2+}-nitrilotriacetic acid sensor chip, and the interaction with fluid-phase inhibitors was subsequently detected. For detection, the inhibitors (analytes) were prepared at various concentrations in 1 × PBS containing 0.5% DMSO and 2% BSA. Throughout the analysis, the chip was regenerated using 10 mM glycine–HCl buffer (pH 2.2 for each experiment. The obtained data were fitted to a 1:1 binding model using Trace Drawer software and the dissociation constant (KD) was determined.

2.4. MD simulations

The structural conformations of the screened inhibitors (ST166, ST132, and ST950) from ligand-pharmacophore (Phar-PR-n4) mapping were investigated using MD simulations. The only direct binding site of the identified inhibitors was the CTD of PhoP (PhoPC); hence, the N-terminal domain of PhoP was removed from the MD simulations. The construction of the protein-ligand complex proceeded as follows. Initially, the conformation of the ligand was acquired from the outcome of ligand-pharmacophore mapping. Subsequently, the ligand fitted to the pharmacophore is relocated within the protein structure, which serves as the basis for generating a pharmacophore model. Before an MD simulation, the complex structures of the protein-ligand were subjected to the “Prepare proteins” method in Discovery Studio 2021 to remove any errors in these structures. Subsequently, the PhoPC–inhibitor complexes were solvated (using Discovery Studio 2021) to create an orthorhombic cell shape under the CHARMm force field, with 0.15 M NaCl added to neutralize the system. Consequently, the PhoPC–inhibitor complex was solvated with water, sodium, and chloride atoms (3053 water molecules, 11 sodium atoms, and 8 chloride atoms for the PhoPC-ST166 complex; 3089 water molecules, 11 sodium atoms, and 8 chloride atoms for the PhoPC-ST132 complex; and 3094 water molecules, 12 sodium atoms, and 9 chloride atoms for the PhoPC-ST950 complex). Energy minimization was then performed for 5000 steps using the steepest descent method, after which an additional 5000 steps were performed using the conjugate gradient method. This was followed by a heating phase of 20 ps and an equilibration phase of 500 ps. This procedure was performed using the Standard Dynamic Cascade protocol in Discovery Studio 2021. After the equilibration process, the entire protein-ligand complex was simulated in a production run of 100 ns executed in the NVT ensemble at 300 K; snapshots were saved every 500 ps. In addition, the Generalized Born algorithm was used for the implicit solvent model during the simulations. The Particle Mesh Ewald (PME) method was used for the electrostatic calculations. Additionally, the SHAKE algorithm was employed to constrain hydrogen-containing bonds (time step = 2 fs). Once the simulation was completed, various parameters were assessed, including the root mean square deviation

(RMSD), root mean square fluctuation (RMSF), and radius of gyration (Rg). The RMSD, RMSF, and Rg values were calculated using the "Analyze Trajectory" protocol of the simulation tool in Discovery Studio 2021. These evaluations were performed with the initial structure as the reference point to examine the conformational changes that occurred within the protein-ligand complexes throughout the simulation.

2.5. Binding free energy calculation

The binding free energy ΔG is a crucial parameter for assessing a compound's affinity for a specific protein[53]. ΔG can be determined using the molecular mechanics Poisson–Boltzmann surface area (MM/PBSA) method. MM/PBSA is a rapid and precise method for predicting the absolute binding affinity of a compound to the active binding site of a target protein, which is crucial for understanding the thermodynamic stability and efficacy of the compound in terms of either inhibition or activation[54]. The binding free energies for each protein-ligand complex were computed using the "Binding Free Energy Single Trajectory" protocol in Discovery Studio 2021. The binding free energy was calculated for all generated conformations to determine the average ΔG for each protein-ligand complex[55].

3. Minimum inhibitory concentration

To assess the susceptibility of *M. marinum* (NTUH-M6885) to antibiotics and ST166, bacterial cells were collected from 7H10 agar plates and resuspended in distilled water to achieve a McFarland standard equivalent of 0.1. Broth microdilution was performed using U-shaped 96-well microtiter plates, with some modifications based on the procedure described by Coban *et al.* [56]. The wells were loaded with 100 μl of 7H9 Broth medium (BD Difco™ & BBL™) supplemented with ADC Enrichment (BD Difco™ & BBL™), and serial dilutions were carried out for each drug. Approximately 5 μl (1.25×10^4 CFU/ml) of bacterial suspension was added to each well. The plates were incubated at 28 °C until bacterial growth was observed in the control medium. Minimum inhibitory concentration (MIC) was defined as the lowest concentration at which no bacterial growth was detected by microscopic examination.

4. Evaluation of cell viability

In 24-well plates, OECM-1 oral cancer cells were seeded with Gibco RPMI-1640 medium containing 10% FBS and antibiotics. These cells were then treated with 0, 50, 100, 127, or 254 μM of ST166 and incubated for 0, 2, or 4 d. After incubation, the supernatant was removed, and the attached cells were washed twice with PBS and stained with 0.23% crystal violet solution (Sigma-Aldrich) for 10 min. After washing twice, the plate was air-dried before further dissolution in a 1% SDS solution. The cell viability was quantified using a microplate reader at 562 nm. The value of the mock control was defined as 100% to calculate the relative cell viability.

5. Results

5.1. Receptor–ligand-pharmacophore generation and pharmacophore-based inhibitor screening

We used the PhoP–DNA complex structure (PDB ID: 5ED4; Figure S1) to construct a pharmacophore model via receptor–ligand-pharmacophore generation, with the PhoP moiety as the receptor and the DNA structure as the ligand. Two clusters of pharmacophore features (models) were generated, Phar-PL and Phar-PR (Fig. 1A). Phar-PL contains seven hydrogen-bond acceptors (green spheres), two hydrogen-bond donors (magenta spheres), and one negatively charged molecule (blue sphere). Phar-PR comprises 11 hydrogen-bond acceptors, two hydrogen-bond donors, and five negatively charged features (Fig. 1A). The choice of pharmacophore scaffold is critical for efficient ligand-pharmacophore mapping and inhibitor screening. A comprehensive exploration of the pharmacophore features of Phar-PL and Phar-PR revealed that four negatively charged features (n1, n2, n3, and n4) represented a bioactive DNA scaffold that interacted with residues R223, S219, R222, T235, Y241, and K195 (Figs. 1B and 1C). These Phar-PR features were further grouped into a pharmacophore scaffold, Phar-PR-n4, and employed to screen potential inhibitors. A compound library comprising 68,000 molecules was obtained from the IBS database. Ligand-pharmacophore mapping was performed to screen and fit the compounds onto Phar-PR-n4. During ligand-pharmacophore mapping, the 3D coordinates of the ligands were aligned to the pharmacophore features of Phar-PR-n4, and the fit between the ligand and pharmacophore was assessed. The following ten compounds with the best fit were selected as candidates (Figure S2): ST166 > ST132 > ST950 > ST142 > ST270 > ST505 > ST439 > ST142 > ST524 > ST272. The detailed chemical structures are shown in Fig. 2.

5.2. Inhibitor disruption of the formation of PhoP- and MtrAC-DNA complexes

The DNA-binding properties of PhoP and MtrAC were characterized to establish an inhibitory assay. The DNA-binding affinity for the

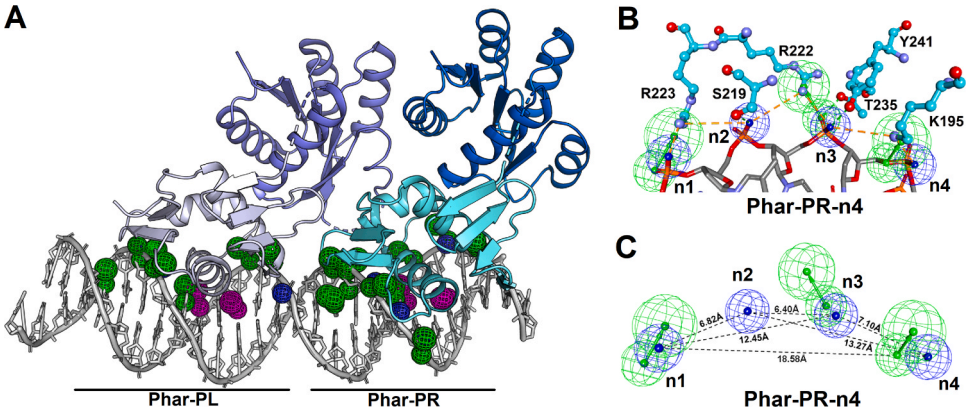

Fig. 1. Receptor–ligand-pharmacophore generation based on the structure of the PhoP–DNA complex. (A) Generated pharmacophore features and structure of the PhoP–DNA complex. (Pharmacophore features are color-coded as follows: hydrogen-bond acceptor, green; hydrogen-bond donor, magenta; negative charge features, deep blue) (B) Pharmacophore scaffold of Phar-PR-n4 aligned with the DNA structure (gray sticks); the interactive residues of PhoP are shown as cyan sticks and labeled. (C) Features at a specific distance correspond to the pharmacophore model Phar-PR-n4. (Pharmacophore features are colored as follows: hydrogen-bond acceptor, green; negative charge, deep blue).

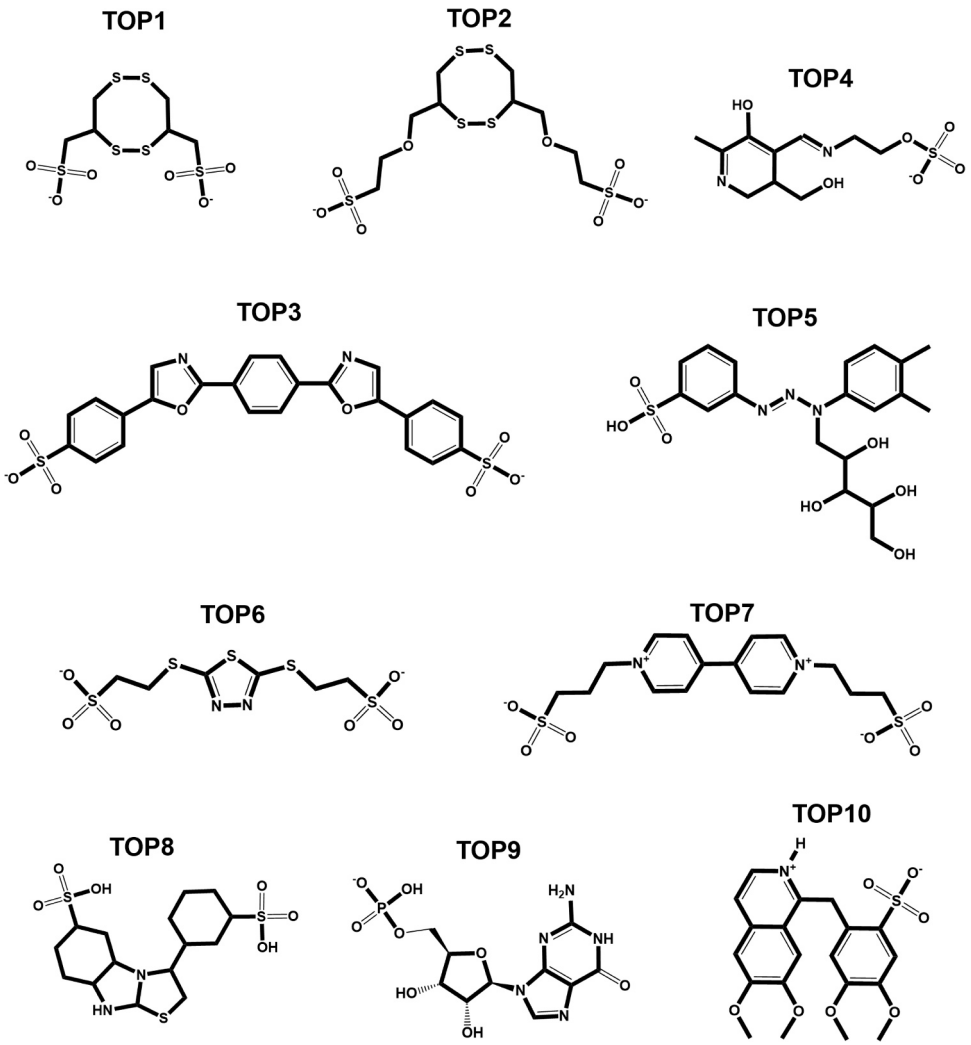

Fig. 2. Chemical structures of the identified top10 ranked hits from pharmacophore-based inhibitor screening.

PhoP–DNA complex was assessed with the DNA sequence (5′-GATTCACAGCTGATTCACAGCATCTA-3′), and the affinity for the MtrAC-DNA complex was assessed with *dnaA* promoter DNA (5′- GGCGGTGTAGTTATCACGCCGTTT-3′) [52] in FP experiments. For PhoP, the polarization intensity increased as the PhoP protein concentration increased (Fig. 3A). However, substantial PhoP aggregation was observed at protein concentrations greater than 50 μM. Hence, 20 μM PhoP was identified as a suitable concentration for further inhibition assays. For MtrAC, strong binding to *dnaA* was observed with a KD value of 1.23 ± 0.26 μM (Fig. 3B). The polarization intensity plateaued for MtrAC concentrations greater than 10 μM; hence, this concentration was used for further inhibition assays. The inhibitory capability of the 10 candidates was then evaluated at a concentration of 100 μM. For PhoP binding to DNA, ST166, ST132, and ST950 showed greater than 50% inhibition (Fig. 4A), ST142 showed approximately 40% inhibition, and ST270, ST505, ST439, ST524, and ST272 showed little to no inhibition (Fig. 4A). For MtrAC binding with DNA, ST166, ST132, and ST142 had over 50% inhibition; the other candidates showed little or no inhibition

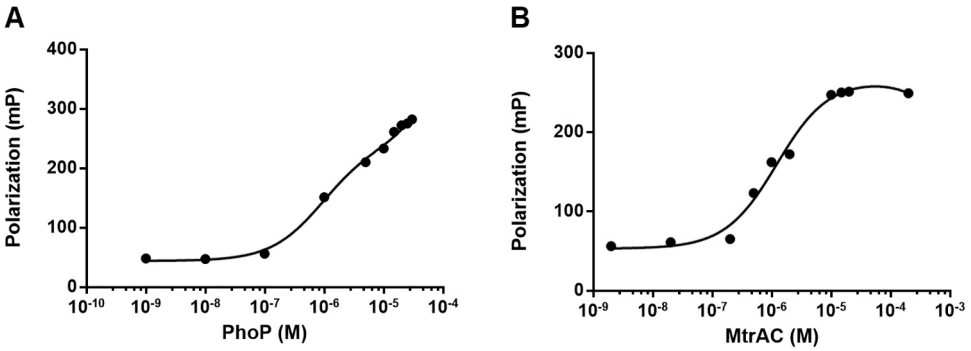

Fig. 3. DNA-binding properties of PhoP and MtrAC. Results of the FP experiments for DNA-binding ability of (A) PhoP and (B) MtrAC as a function of protein concentration. For MtrAC, the determined KD was 1.23 ± 0.26 μM.

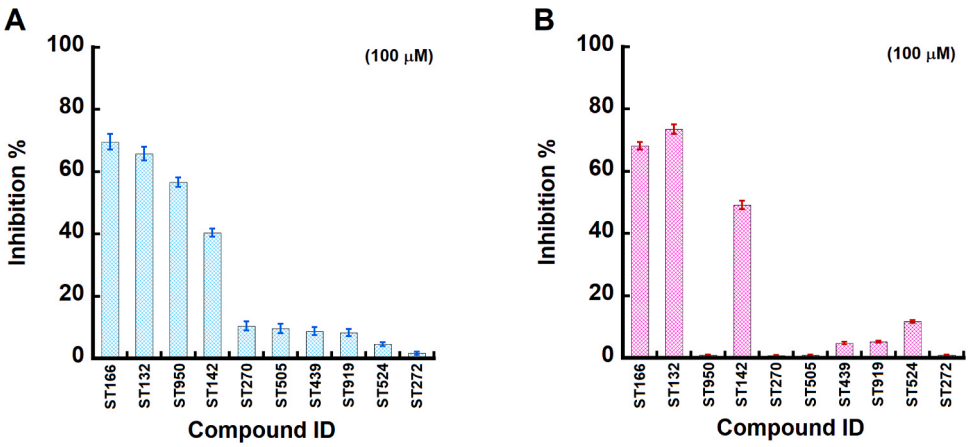

Fig. 4. Inhibitory potency of the 10 best candidates against PhoP and MtrAC for DNA binding. Inhibitory ability of the 10 hits against formation of the (A) PhoP–DNA and (B) MtrAC-DNA complexes at 100 μM.

(Fig. 4B). Candidates with > 50% inhibition were investigated in inhibitory experiments using a series of compound concentrations to determine the IC_{50} values. For PhoP binding with DNA, ST166, ST132, and ST950 had dose-dependent inhibition, with IC_{50} values of 18 ± 1.3, 29 ± 1.6, and 88 ± 1.2 μM, respectively (Fig. 5A). Likewise, for ST166 and ST132 against MtrAC binding with DNA, the IC_{50} was 24 ± 1.1 and 48 ± 0.8 μM (Fig. 5B), respectively; the IC_{50} of ST950 could not be determined.

5.3. MD simulations and MMPBSA-based binding free energy

MD simulations were performed to determine binding of the inhibitor to the C-terminal DBD of PhoP (PhoPC). The average RMSD, RMSF, and Rg of PhoPC-ST166, PhoPC-ST132, and PhoPC-ST950 for all conformations were calculated through simulations with a duration of 100 ns and compared with those of the control (PhoPC alone) to determine the stability of the complexes. The average RMSD for PhoPC alone was 1.35 Å, smaller than that of the PhoPC-ST166 complex (1.86 Å; Fig. 6A). However, the RMSD was higher for PhoPC-ST132 and PhoPC-ST950, equal to 2.10 and 2.81 Å, respectively. Fluctuations in individual residues within the simulation period are plotted in Fig. 6B. The residues for PhoPC and PhoPC-ST166 had similar RMSF patterns, but those of the PhoPC-ST132 and PhoPC-ST950 complexes differed greatly, suggesting that these ligands affected the stability of PhoPC and altered its dynamic behavior. Only the Rg for PhoPC was stable, and fluctuated slightly between 13.03–13.16 Å (Fig. 6C). Similarly, for PhoPC-ST166, Rg fluctuated slightly between 13.09–13.24 Å. By contrast, Rg fluctuated substantially for the PhoPC-ST132 and PhoPC-ST950 complexes between 12.93–13.31 and 13.03–13.50 Å, respectively. In addition, ligand RMSD revealed the stable binding of ST166 to the target proteins (Fig. 6D). Moreover, the average free energy of PhoPC binding for each protein-ligand complex was determined using the MM-PBSA method as − 13.9, 6.5, and 3.7 kcal/mol for ST166, ST132, and ST950, respectively (Fig. 6E). Hence, ST166 formed a thermodynamically stable complex with PhoPC, whereas complexes with ST132 and ST950 were less stable.

5.4. Analyses of molecular interactions of inhibitors with PhoPC

To better understand the molecular interactions between the identified inhibitors—ST166, ST132, and ST950— and PhoPC, structural analyses were performed using the non-bond interaction analysis module in Discovery Studio 2021. The conformations of ST166, ST132, and ST950 in complex with PhoPC were obtained at MD simulation time points of 10 and 100 ns. ST166, ST132, and ST950 bound to the DNA-binding region of PhoPC at distinct positions and orientations by interacting with functionally essential residues (Fig. 7). ST166, ST132, and ST950 also interacted with the DNA-binding residues of PhoPC through various charge–charge interactions, hydrogen bonding, and hydrophobic contacts (Fig. 7). At a simulation time of 10 ns, ST166 interacted with PhoP through seven hydrogen bonds, two charge–charge interactions, and one sulfur–x interaction (Fig. 7A). At the same time point, ST132 was bound to PhoPC with six hydrogen bonds, two charge–charge interactions, one π–anion interaction, and one hydrophobic

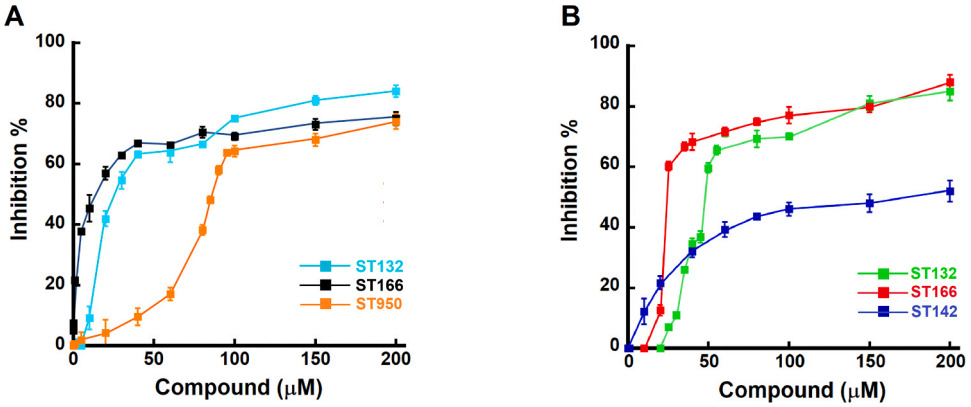

Fig. 5. Inhibitory potencies of ST166, ST132, ST950, and ST142 as a function of compound concentration. (A) Dose-dependent inhibition curves of ST166, ST132, and ST950 against the formation of PhoP–DNA complex. (B) Dose-dependent inhibition curves of ST166, ST132, and ST142 against the formation of MtrAC-DNA complex.

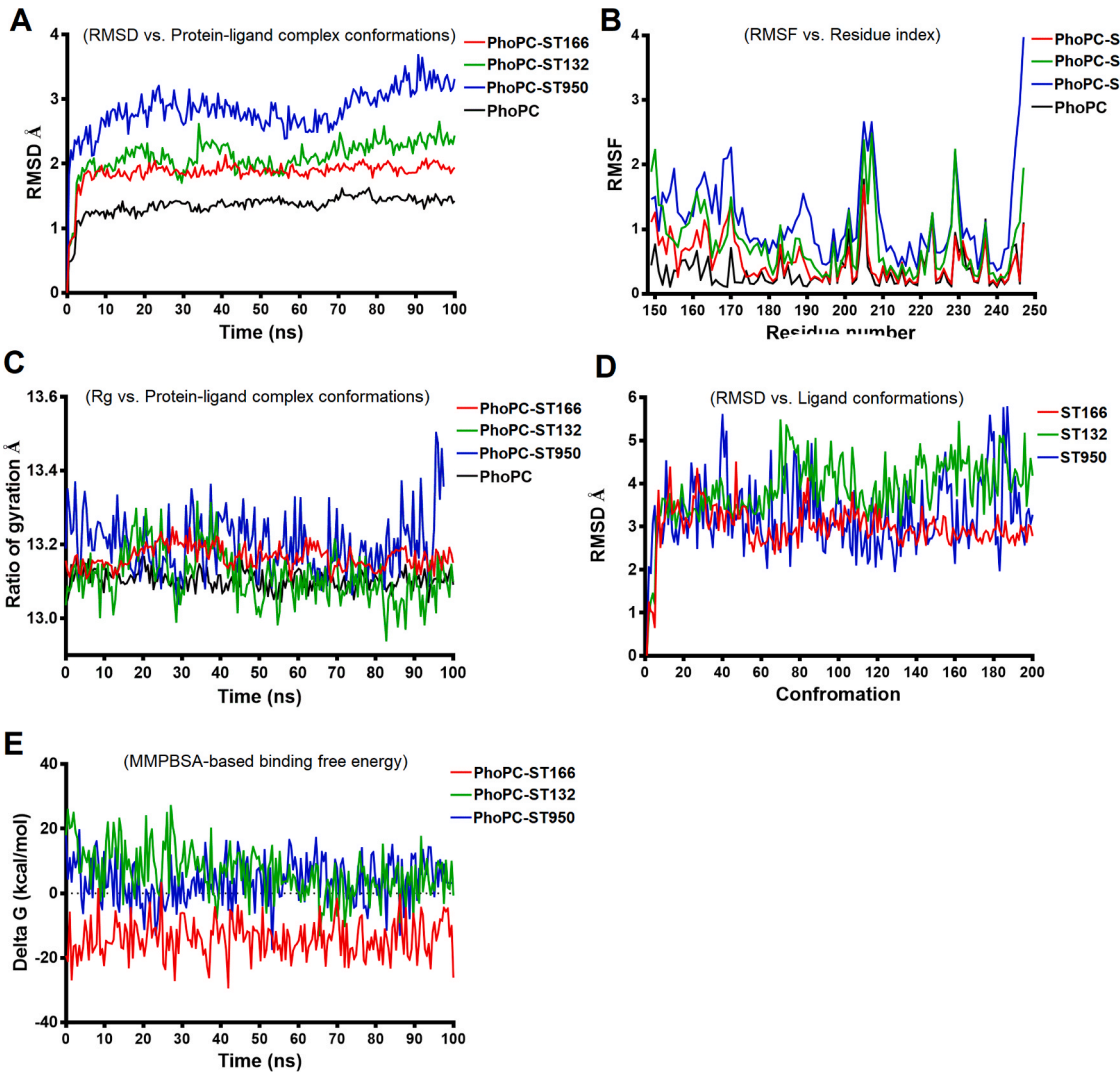

Fig. 6. Stability parameters obtained from the MD simulation analysis and binding free energy. (A) RMSD of protein-ligand complexes as a function of simulation time. (B) RMSF values of the PhoPC residues. (C) Rg values as a function of simulation time. (D) RMSD of ligands as a function of simulation time. (E) Free binding energies for each protein–inhibitor complex, obtained through MM-PBSA.

contact (Fig. 7B). In contrast, ST950 interacted with PhoPC through four hydrogen bonds, two charge–charge interactions, and one hydrophobic contact (Fig. 7C).

5.5. PhoP and MtrAC binding affinities of ST166 and ST132

In our pharmacophore-based inhibitor screen, we identified ST166 and ST132 as strong inhibitors of PhoP and MtrAC, respectively. To confirm the interactions of these inhibitors with MtrAC and PhoP, their binding affinities were investigated by LSPR. First, the binding of MtrAC to DNA was verified; the determined KD value was 1.4 ± 0.3 μM (Fig. 8A). The binding of ST132 to MtrAC was investigated at ST132 concentrations of 12.5, 25, and 50 μM. The K_{on} and K_{off} rates were determined to be $3.2 \times 10^3 \pm 5.2 \times 10^2$ (M^{-1} s^{-1}) and $2.7 \times 10^{-2} \pm 7.5 \times 10^{-4}$ (s^{-1}), individually, which reveals an interaction between ST132 and MtrAC using a slow-on-slow-off binding mechanism (KD = 8.5 ± 0.8 μM; Fig. 8B). The inhibitor ST166 was also tested at concentrations of 12.5, 25, and 50 μM in the LSPR experiments. The result showed that The SPR signal increased as the concentration of ST166 increased, thereby indicating its binding to MtrAC. The resultant K_{on} and K_{off} rates were determined to be $2.9 \times 10^3 \pm 1.3 \times 10^2$ (M^{-1} s^{-1}) and $1.6 \times 10^{-2} \pm 1.7 \times 10^{-4}$($s^{-1}$), respectively. The sensorgrams indicated slow association and slow dissociation for the binding of ST166 with MtrAC, resulting in a KD value of 5.6 ± 1.2 μM (Fig. 8C). For PhoP, the inhibitor ST132 was assessed at concentrations of 12.5, 25, 50 100 and 150 μM (Fig. 8E). The determined K_{on} was $5.3 \times 10^3 \pm 5.1 \times 10^2$ (M^{-1} s^{-1}), and the K_{off} rate was $7.7 \times 10^{-2} \pm 3.1 \times 10^{-3}$ (s^{-1}), thereby resulting in a KD of 14.5 ± 0.1 μM. For ST166 binding with PhoP, slow association and dissociation were again observed, with KD = 18.4 ± 4.3 μM ($K_{on} = 24.6 \times 10^2 \pm 1.1 \times 10^3$ (M^{-1} s^{-1}) and $K_{off} = 4.5 \times 10^{-3} \pm 1.4 * 10^{-5}$ (s^{-1}) (Fig. 8F).

5.6. Antibacterial activity and cytotoxicity of ST166

The biological activity of ST166 toward *M. marinum* was assessed to determine its MIC. ST166 inhibited the growth of *M. marinum* with an MIC of greater than 128 μg/ml (254 μM) (Figure S3A). For comparison, established drugs, such as ciprofloxacin and rifampicin, have MIC values of 8 and 2 μg/ml (24.1 and 2.43 μM), respectively (Figure S3B). The safety profile of ST166 as a drug for the treatment of *Mycobacterium* species infection was investigated. OECM-1 oral cancer cells were treated with 0, 2 50, 100, 127, or 254 μM ST166 for 0, 2, or 4 d. Treatment with ST166 for 4 d did not significantly affect the cells' viability when the ST166 concentration was 50 or 100 μM but resulted in decreased cell viability after 4 d when the ST166 concentration was 127 or 254 μM (viability of 59.8% and 32.5%, respectively; Fig. 9).

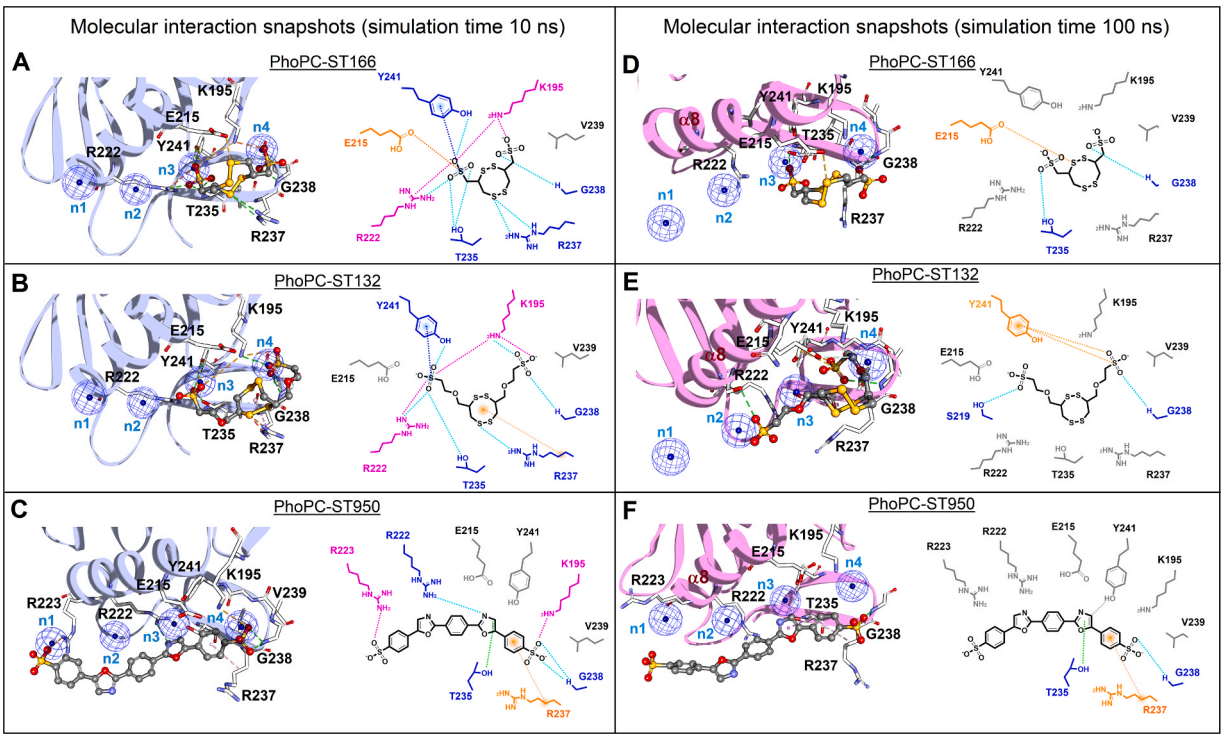

Fig. 7. Molecular interactions of ST166, ST132, and ST950 with PhoPC. Molecular interactions of (A) ST166, (B) ST132, and (C) ST950 with PhoPC from MD simulations at the 10 ns time point and the corresponding interactions for (D) ST166, (E) ST132, and (F) ST950 at the 100 ns time point. In all three-dimensional structural plots, ST166, ST132, and ST950 are presented as sticks (gray); PhoPC is shown as ribbons (light blue and pink); and interactive residues are displayed as white sticks and labeled. In all two-dimensional schematic plots, the chemical structures of the inhibitors are black, the interactive residues of PhoPC are labeled, and the cyan, orange, magenta, green, and red dashed lines indicate hydrogen bonding, hydrophobic interactions, charge–charge interactions, carbon hydrogen bonds, and sulfur–x interactions, respectively.

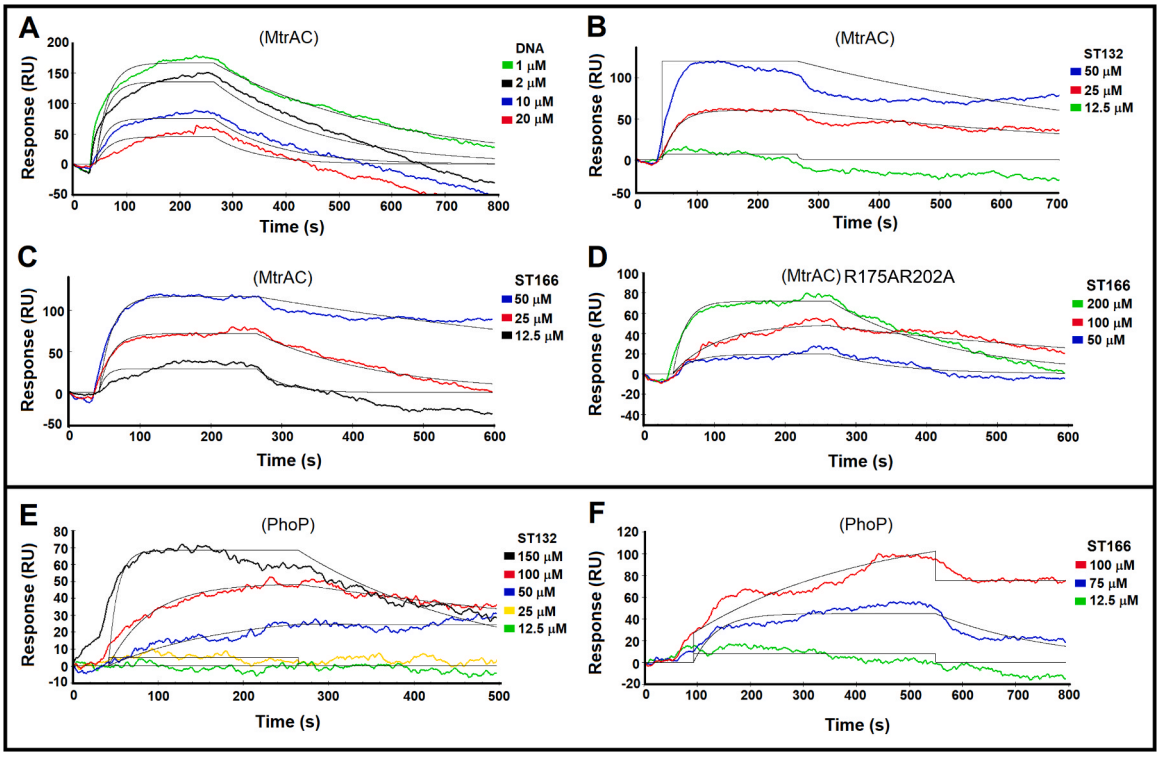

Fig. 8. SPR sensorgrams of ST166 and ST132 binding with PhoP and MtrAC. Binding affinity of (A) MtrAC to DNA (KD = 1.4 ± 0.3 μM), (B) ST132 to MtrAC (KD = 8.5 ± 0.8 μM), (C) ST166 to MtrAC (KD = 5.6 ± 1.2 μM), (D) ST166 to MtrAC-R175AR202A (KD = 34.2 ± 3.7 μM), (E) ST132 to PhoP (KD = 14.5 ± 0.1 μM), and (F) ST166 to PhoP (KD = 18.4 ± 4.3 μM).

These results revealed the cytotoxicity of ST166 in mammalian cells.

6. Discussion

Antibiotic resistance in pathogenic bacteria [57] is a global health concern, especially with the rise of MDR strains including *Mycobacterium tuberculosis* (*Mtb*)[58–60]. Novel strategies to combat this are necessary, such as disrupting bacterial TCSs to reduce biofilm formation, virulence, and antibiotic resistance [77–84]. The development of HK inhibitors has been hindered by their poor bioavailability due to their hydrophobic properties[61–63]. Some inhibitors lack selectivity [64,65] and influence protein aggregation instead of HK inhibition[66]. Targeting the RR is preferable because it can directly interfere with bacterial gene expression and behavior[67]. The RRs MtrA and PhoP mainly control the virulence and antibiotic resistance of *Mtb* [32,68,69], and their simultaneous disruption can compromise the multidrug resistance of *Mtb*. In this study, we aimed to develop potent inhibitors concurrently targeting PhoP and MtrA of *Mtb*, and attempted to achieve this by employing CADD coupled with biochemical and biophysical examinations.

Inhibition of the C-terminal DBD of RRs is a practical strategy for disrupting RR–DNA complex formation because DBDs have well-defined binding sites that can be targeted by small molecules. Pharmacophore modeling is a powerful tool for exploring the functional requirements of receptor–ligand interactions, with specific applications in protein–small molecule and protein–protein complexes[70]. Construction of a pharmacophore model of the essential features of ligand binding to the target protein enabled the identification of potential inhibitors through virtual high-throughput screening. We utilized pharmacophore approaches to explore the bioactive pharmacophore scaffold of the PhoP–DNA complex and applied it to screen potential inhibitors. We rationally generated pharmacophore feature clusters Phar-PL and Phar-PR based on the left and right structural moieties, respectively (Fig. 1). Despite identical PhoP moieties in the left and right parts of the PhoP–DNA complex, the numbers and chemical properties of the pharmacophore features in Phar-PL and Phar-PR differ. This could be due to the distinct molecular interactions between PhoP and the asymmetrical DNA sequence (3′-ATCTACGACACTTAGTCGACACTTAG-5′). Moreover, the novel pharmacophore scaffold with four negatively charged groups (n1–n4), Phar-PR-n4, strongly contributed to PhoP-targeting DNA via electrostatic interactions. ST166, ST132, and ST950 were identified by ligand-pharmacophore mapping and were found to favorably match Phar-PR-n4 (Figure S2). Other candidates (ST270, ST505, ST439, and ST142) were aligned with only two or even one negatively charged feature (ST142, ST524, and ST272), thereby resulting in less favorable poses and lower fit values (Figure S2). Functionally, ST166 had the highest potency against formation of the PhoP–DNA complex (IC_{50} = 18 ± 1.3 μM), followed by ST132 with moderate inhibition (IC_{50} = 29 ± 1.6 μM) and ST950 with minor potency (IC_{50} = 88 ± 1.2 μM). These observations corroborated the ligand-pharmacophore mapping fitness results of ST166 (fit value = 4.50), ST132 (fit value = 4.36), and ST950 (fit value = 3.71; Figure S2). These findings confirmed the utility and reliability of the pharmacophore model Phar-PR-n4 for screening targeted inhibitors of PhoP–DNA complex formation.

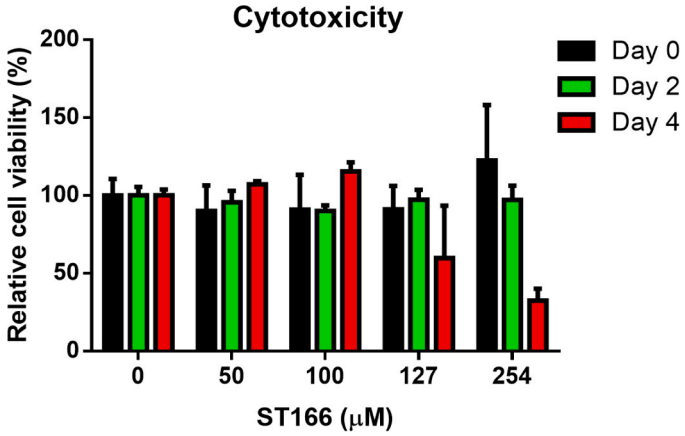

Fig. 9. Cell viability of OECM-1 under ST166 treatment.

To gain insight into the binding dynamics of PhoPC with the inhibitors ST132, ST166, and ST950, we performed 100-ns MD simulations to assess the stability of the complexes in terms of the key metrics RMSD, RMSF, and Rg (Fig. 6) in comparison with a control (PhoPC alone). The average RMSD for PhoPC alone was 1.35 Å; that for the PhoPC-ST166 complex was slightly greater (1.86 Å), and those for the PhoPC-ST132 and PhoPC-ST950 indicated greater deviations (Fig. 6A). This suggests that the inhibitors ST132 and ST950 reduce the stability and alter the dynamic behavior of PhoPC. The RMSF patterns of PhoPC and PhoPC-ST166 residues were highly similar, but those of PhoPC-ST132 and PhoPC-ST950 complexes differed significantly (Fig. 6B). Regarding the analysis of Rg, which indicates the structural stability during the simulation, PhoPC and PhoPC-ST166 were found to be the most stable, with Rg values of 13.03–13.24 Å; PhoPC-ST132 and PhoPC-ST950 had fluctuating Rg values of 12.93–13.31 and 13.03–13.50 Å, respectively (Fig. 6C). These findings implied that the introduction ST132 or ST950 led to pronounced changes in the overall structure and shape of the complex. The MM-PBSA calculations of the binding free energy also indicated that the PhoPC-ST166 complex was the most stable (−13.9 kcal/mol vs 6.5 and 3.7 kcal/mol for ST132 and ST950, respectively; Fig. 6E). Thus, ST166 formed the most thermodynamically stable complex with PhoPC. MD simulations and binding free energy calculations provide a detailed understanding of the dynamic and thermodynamic aspects of the interactions between inhibitors and PhoPC, revealing the stability and behavior of these complexes for future drug design and experimental investigations.

The atomic interactions of ST166, ST132, and ST950 with PhoPC were explored in detail using non-bonding interaction analyses. At a simulation time of 10 ns, ST166 was found to bind to PhoPC through charge–charge interactions, in which its two sulfonic groups interacted with residues R222 and K195 (Fig. 7A). ST166 also established a hydrogen-bond network with residues T235, R237, G238, and Y241, and the sulfonic group on its left side engaged in a π–sulfur interaction with residue Y241 (Fig. 7A). In addition, one sulfur atom on the tetrathiocane of ST166 interacted with E215 through a sulfur–x interaction, reinforcing the stability of the PhoPC-ST166 complex. These interactions, coupled with the previously discussed hydrogen bonds and electrostatic interactions, underscore the structural compatibility of ST166 with part of the DNA-binding site of PhoPC, thereby leading to significant inhibitory effectiveness. At a simulation time of 100 ns, a sulfur–x interaction and two hydrogen bonds remained, maintaining the interaction of ST166 with PhoPC (Fig. 7D). At the time point of 10 ns, non-bonding interaction analysis of ST132 revealed electrostatic interactions with residues R222 and K195 through its terminal sulfonic groups (Fig. 7B). ST132 also formed a hydrogen-bond network with PhoPC through the same residues as ST166 (T235, R237, G238, and Y241), strengthened by hydrophobic interactions with residue R237. However, unlike ST166, ST132 lacked a sulfur–x interaction with E215 (Fig. 7B). The differences in the molecular interactions of ST166 and ST132 with PhoPC explain the lower efficacy of ST132 against PhoP–DNA complex formation. As the simulation time increased to 100 ns, residues Y241 (π–anion), S219 (hydrogen bond), and G238 (hydrogen bond) of PhoPC remained mostly in contact and bound with ST132 (Fig. 7E). ST166 and ST132 have structural similarities but both differ considerably from ST950 (Fig. 2). Structurally, the core of ST166 and ST132 comprises 1,2,5,6-tetrathiocane (Fig. 2). Modifying the 3 and 8 positions of the central core with ethanesulfonates forms the chemical structure of ST166 (Fig. 2), whereas modification with 2-

propoxyethanesulfonate at the 3 and 8 positions forms the structure of ST132. The chemical structure of ST950 consists of two benzene rings with attached sulfonic groups connected to a central core containing a phenylene group connected to two oxazole rings. ST166, ST132, and ST950 have two sulfonic groups that resemble the functional phosphate groups of DNA, which electrostatically interact and bind with PhoP. Structurally, the sulfonic groups of ST950 interact electrostatically with residues R223 and K195 of PhoP. However, the hydrogen-bond network in ST950 was less organized and involved residues R222, G238, and T235 (Fig. 7C). Although R237 engaged in hydrophobic contact with one of the benzene rings of ST950, it did not participate in hydrogen bonding. Therefore, the structure of ST950 is larger and longer, and the interactions of ST950 with PhoP are insufficient to stabilize the whole complex, resulting in ST950 having a lower inhibitory potency than ST166 and ST132.

Sequence alignment of the RRs revealed high similarities among PhoP, MtrA, PrrA, and RegX3 of *Mtb* (Figure S4). Specifically, the C-terminal DBD of PhoP had 57.9%, 59.2%, and 56.3% sequence similarity with MtrA, PrrA, and RegX3, respectively (Figure S4A). The DBDs of PhoP, MtrA, and PrrA are structurally similar (Figure S4B). This conserved region included essential DNA-binding residues (K195, E215, R222, R223, T235, and Y241) in PhoP; the corresponding residues in MtrA and PrrA are highlighted in Figure S4B. These observations suggest that ST166, ST132, and ST950 target MtrA, PrrA, and RegX3, potentially disrupting their DNA-binding abilities. The in vitro inhibition assay showed that ST166 and ST132 exhibited similar inhibitory effects on MtrAC and PhoP for DNA binding (Fig. 5), whereas ST950 specifically affected PhoP, but not MtrAC. Further investigation revealed that ST166 inhibited MtrAC in a dose-dependent manner, with an IC_{50} value of 48 $\pm$ 0.8 μM. ST132 moderately inhibited MtrAC with an IC_{50} of 24 $\pm$ 1.1 μM. In contrast, ST166 (IC_{50} = 18 $\pm$ 1.3 μM) and ST132 (IC_{50} = 29 $\pm$ 1.6 μM) exhibited strong inhibitory effects against PhoP. To understand these variations, a detailed structural comparison was performed (Figure S5). The structures of ST166 and ST132 complexed with PhoPC (from MD simulations) overlapped with those of MtrAC, which reveals differences between PhoPC-ST166 and MtrAC (Figure S5A–C). Specifically, E215 of PhoPC forms a sulfur–x interaction with the middle ring of ST166, whereas N195 of MtrAC interacts with the sulfur atom through hydrogen bonding. Additionally, R237 and G238 of PhoPC interacted with ST166 through hydrogen bonds, whereas the side chain of R219 and main chain of G220 of MtrAC did not form hydrogen bonds with ST166 because they were positioned farther away. In the superimposition of PhoPC-ST132 with MtrAC (Figure S5D–F), the interactions observed between ST132 and R237 and G238 in PhoPC were lost because ST132 came into proximity with the corresponding residues R219 and G220 of MtrAC. These variations in the molecular interactions of ST166 and ST132 with PhoPC and MtrAC accounted for their distinct inhibitory potencies. To confirm the proposed binding sites of ST166 and ST132, we performed MtrAC mutagenesis (see Supporting Information and Table S1). In the MtrAC-ST166 complex, residues R175 and R202 interacted with ST166 via hydrogen bonding (Figure S5C). To confirm these interactions, residues R175 and R202 were mutated to alanine and subjected to LSPR to evaluate changes in binding affinity. The results showed that ST166 exhibited weaker binding to the variant MtrAC-R175AR202A (KD = 34.2 $\pm$ 3⊡7 μM; Fig. 8D) compared with the wild type MtrAC (KD = 5.6 $\pm$ 1.2 μM). This indicates that the binding sites for ST166 and ST132 could be located near residues R175 and R202 on MtrAC, consistent with our modeled protein–inhibitor complex structures. Moreover, the lack of inhibitory activity of ST950 against formation of the MtrAC-DNA complex is noteworthy given that ST950 was the most effective in reducing PhoP–DNA complex formation by at least 40% when used at a concentration of 100 μM. In the PhoPC-ST950 complex structure, the terminal sulfonic groups of ST950 were anchored by residues R223 and K195, whereas the oxazole and benzene rings on the right side interacted with residues R222, T235, R237, and G238 (Figure S5G–I). However, in its interactions with MtrAC, ST950 forms only one connection with a terminal sulfonic group tethered to residue R175. The differences in these interactions stem from variations in the side-chain residues, thereby highlighting the importance of these variations in the effectiveness of ST950.

7. Conclusion

We employed a comprehensive approach that combined pharmacophore-based inhibitor screening with biochemical and biophysical examinations to identify, characterize, and validate potential inhibitors targeting PhoP and MtrA in *Mtb*. Using the pharmacophore model Phar-PR-n4, we conducted ligand-pharmacophore mapping of 68,000 compounds and identified ST166 and ST132 as promising inhibitors that disrupt the formation of PhoP- and MtrA-DNA complexes. We demonstrated that ST166 and ST132 interact with PhoP and MtrAC in a slow-on-slow-off manner. The modeled complex structure revealed that ST166 and ST132 mainly interact with the α8-helix and C-terminal β-hairpin of the DBD, and the conserved and functionally essential residues are hotspots for further structure-based inhibitor optimization. Our study demonstrated the application of the protein–DNA complex structure to generate a pharmacophore model and the use of this model to discover inhibitors with high inhibitory potency and binding affinity that target the RRs of *Mtb* PhoP and MtrA. ST166, characterized by its terminal sulfonic and oxazole groups, showed in vitro antibacterial activity against *Macrobacterium marinum* and could serve as a starting point for the development of new antimicrobial agents.

CRediT authorship contribution statement

Tien-Sheng Tseng: Writing – review & editing, Writing – original draft, Visualization, Validation, Supervision, Software, Resources, Project administration, Methodology, Investigation, Funding acquisition, Formal analysis, Data curation, Conceptualization. **Han-Li Su:** Validation, Methodology, Investigation, Data curation. **Shu-Jung Lai:** Validation, Methodology, Investigation, Data curation. **Keng-Chang Tsai:** Validation, Methodology, Investigation, Data curation. **Kit-Man Fung:** Validation, Methodology, Data curation. **Tse-Lin Lung:** Validation, Investigation, Data curation. **Hsing-Mien Hsu:** Validation, Investigation, Data curation. **Yi-Chen Wu:** Investigation, Data curation. **Ching-Hui Liu:** Validation, Data curation. **Hui-Xiang Lai:** Validation. **Jiun-Han Lin:** Validation, Data curation.

Declaration of Competing Interest

There are no conflicts of interest to declare.

Acknowledgements

We thank the National Center for High-Performance Computing for providing computational and storage resources. This study was supported by the National Science and Technology Council of Taiwan (grant numbers NSTC-111-2311-B-005-006 and NSTC 112-2320-B-005-010-MY3). This study was financially supported in part by a grant from the Ditmanson Medical Foundation, Chia-Yi Christian Hospital, to Tien-Sheng Tseng and Han-Li Su (CYCH-NCHULS111005).

Appendix A. Supporting information

Supplementary data associated with this article can be found in the online version at doi:10.1016/j.csbj.2024.04.005.

References

[1] Smith I. Mycobacterium tuberculosis pathogenesis and molecular determinants of virulence. Clin Microbiol Rev 2003;16:463–96. https://doi.org/10.1128/CMR.16.3.463-496.2003.

[2] Zhang T, Zhang J, Wei L, Liang H, Zhang J, et al. The global, regional, and national burden of tuberculosis in 204 countries and territories, 1990-2019. J Infect Public Health 2023;16:368–75. https://doi.org/10.1016/j.jiph.2023.01.014.

[3] Goletti D, Pisapia R, Fusco FM, Aiello A, Van Crevel R. Epidemiology, pathogenesis, clinical presentation and management of TB in patients with HIV and diabetes. Int J Tuberc Lung Dis 2023;27. https://doi.org/10.5588/ijtld.22.0685.

[4] Park M, Satta G, Kon OM. An update on multidrug-resistant tuberculosis. Clin Med (Lond) 2019;19:135–9. https://doi.org/10.7861/clinmedicine.19-2-135.

[5] Betts JC, Lukey PT, Robb LC, McAdam RA, Duncan K. Evaluation of a nutrient starvation model of Mycobacterium tuberculosis persistence by gene and protein expression profiling. Mol Microbiol 2002;43:717–31. https://doi.org/10.1046/j.1365-2958.2002.02779.x.

[6] Fisher MA, Plikaytis BB, Shinnick TM. Microarray analysis of the Mycobacterium tuberculosis transcriptional response to the acidic conditions found in phagosomes. J Bacteriol 2002;184:4025–32. https://doi.org/10.1128/jb.184.14.4025-4032.2002.

[7] Via LE, Lin PL, Ray SM, Carrillo J, Allen SS, et al. Tuberculous granulomas are hypoxic in guinea pigs, rabbits, and nonhuman primates. Infect Immun 2008;76:2333–40. https://doi.org/10.1128/IAI.01515-07.

[8] Voskuil MI. Mycobacterium tuberculosis gene expression during environmental conditions associated with latency. Tuberc (Edinb) 2004;84:138–43. https://doi.org/10.1016/j.tube.2003.12.008.

[9] Wayne LG, Hayes LG. An in vitro model for sequential study of shiftdown of Mycobacterium tuberculosis through two stages of nonreplicating persistence. Infect Immun 1996;64:2062–9.

[10] Stock AM, Robinson VL, Goudreau PN. Two-component signal transduction. Annu Rev Biochem 2000;69:183–215. https://doi.org/10.1146/annurev.biochem.69.1.183.

[11] Gao R, Mack TR, Stock AM. Bacterial response regulators: versatile regulatory strategies from common domains. Trends Biochem Sci 2007;32:225–34. https://doi.org/10.1016/j.tibs.2007.03.002.

[12] Gao R, Stock AM. Biological insights from structures of two-component proteins. Annu Rev Microbiol 2009;63:133–54. https://doi.org/10.1146/annurev.micro.091208.073214.

[13] Gao R, Stock AM. Molecular strategies for phosphorylation-mediated regulation of response regulator activity. Curr Opin Microbiol 2010;13:160–7. https://doi.org/10.1016/j.mib.2009.12.009.

[14] Stock AM, West AH. Response regulator proteins and their interactions with histidine protein kinases. New York: Academic Press,; 2003.

[15] Rasko DA, Moreira CG, Li De R, Reading NC, Ritchie JM, et al. Targeting QseC signaling and virulence for antibiotic development. Science 2008;321(1979):1078–80. https://doi.org/10.1126/science.1160354.

[16] Shakhnovich EA, Hung DT, Pierson E, Lee K, Mekalanos JJ. Virstatin inhibits dimerization of the transcriptional activator ToxT. Proc Natl Acad Sci USA 2007;104(7):2372. https://doi.org/10.1073/pnas.0611643104.

[17] Hung DT, Shakhnovich EA, Pierson E, Mekalanos JJ. Small-molecule inhibitor of Vibrio cholerae virulence and intestinal colonization. Science 2005;310(1979):670–4. https://doi.org/10.1126/science.1116739.

[18] Gotoh Y, Eguchi Y, Watanabe T, Okamoto S, Doi A, et al. Two-component signal transduction as potential drug targets in pathogenic bacteria. Curr Opin Microbiol 2010;13:232–9. ⟨https://doi.org/10.1016/j.mib.2010.01.008⟩.

[19] Tang YT, Gao R, Havranek JJ, Groisman EA, Stock AM, et al. Inhibition of bacterial virulence: drug-like molecules targeting the Salmonella enterica PhoP response regulator. Chem Biol Drug Des 2012;79:1007–17. https://doi.org/10.1111/j.1747-0285.2012.01362.x.

[20] Ma C, Yang X, Kandemir H, Mielczarek M, Johnston EB, et al. Inhibitors of bacterial transcription initiation complex formation. ACS Chem Biol 2013;8:1972–80. https://doi.org/10.1021/cb400231p.

[21] Harris TL, Worthington RJ, Hittle LE, Zurawski DV, Ernst RK. Small molecule downregulation of PmrAB reverses lipid A modification and breaks colistin resistance. ACS Chem Biol 2014;9:122–7. https://doi.org/10.1021/cb400490k.

[22] Zahrt TC, Deretic V. An essential two-component signal transduction system in Mycobacterium tuberculosis. J Bacteriol 2000;182:3832–8. https://doi.org/10.1128/jb.182.13.3832-3838.2000.

[23] Fol M, Chauhan A, Nair NK, Maloney E, Moomey M, et al. Modulation of Mycobacterium tuberculosis proliferation by MtrA, an essential two-component response regulator. Mol Microbiol 2006;60:643–57. https://doi.org/10.1111/j.1365-2958.2006.05137.x.

[24] Rajagopalan M, Dziedzic R, Al Zayer M, Stankowska D, Ouimet MC, et al. Mycobacterium tuberculosis origin of replication and the promoter for immunodominant secreted antigen 85B are the targets of MtrA, the essential response regulator. J Biol Chem 2010;285:15816–27. https://doi.org/10.1074/jbc.M109.040097.

[25] Nguyen HT, Wolff KA, Cartabuke RH, Ogwang S, Nguyen L. A lipoprotein modulates activity of the MtrAB two-component system to provide intrinsic multidrug resistance, cytokinetic control and cell wall homeostasis in Mycobacterium. Mol Microbiol 2010;76:348–64. https://doi.org/10.1111/j.1365-2958.2010.07110.x.

[26] Gorla P, Plocinska R, Sarva K, Satsangi AT, Pandeeti E, et al. MtrA Response Regulator Controls Cell Division and Cell Wall Metabolism and Affects Susceptibility of Mycobacteria to the First Line Antituberculosis Drugs. Front Microbiol 2018;9:2839. https://doi.org/10.3389/fmicb.2018.02839.

[27] Banerjee SK, Kumar M, Alokam R, Sharma AK, Chatterjee A, et al. Targeting multiple response regulators of Mycobacterium tuberculosis augments the host immune response to infection. Sci Rep 2016;6:25851. https://doi.org/10.1038/srep25851.

[28] Peterson EJR, Brooks AN, Reiss DJ, Kaur A, Do J, et al. MtrA modulates Mycobacterium tuberculosis cell division in host microenvironments to mediate intrinsic resistance and drug tolerance. Cell Rep 2023;42. https://doi.org/10.1016/j.celrep.2023.112875.

[29] Ryndak M, Wang S, Smith I. PhoP, a key player in Mycobacterium tuberculosis virulence. Trends Microbiol 2008;16:528–34. https://doi.org/10.1016/j.tim.2008.08.006.

[30] Walters SB, Dubnau E, Kolesnikova I, Laval F, Daffe M, et al. The Mycobacterium tuberculosis PhoPR two-component system regulates genes essential for virulence and complex lipid biosynthesis. Mol Microbiol 2006;60:312–30. https://doi.org/10.1111/j.1365-2958.2006.05102.x.

[31] Gonzalo-Asensio J, Soto CY, Arbues A, Sancho J, del Carmen Menendez M, et al. The Mycobacterium tuberculosis phoPR operon is positively autoregulated in the virulent strain H37Rv. J Bacteriol 2008;190:7068–78. https://doi.org/10.1128/JB.00712-08.

[32] Banerjee SK, Kumar M, Alokam R, Sharma AK, Chatterjee A, et al. Targeting multiple response regulators of Mycobacterium tuberculosis augments the host immune response to infection. Sci Rep 2016;6:25851. https://doi.org/10.1038/srep25851.

[33] Kapetanovic IM. Computer-aided drug discovery and development (CADDD): in silico-chemico-biological approach. Chem Biol Inter 2008;171:165–76. https://doi.org/10.1016/j.cbi.2006.12.006.

[34] Nascimento IJ dos S, de Aquino TM, da Silva-Júnior EF. The New Era of Drug Discovery: The Power of Computer-aided Drug Design (CADD). Lett Drug Des Discov 2022;19. https://doi.org/10.2174/1570180819666220405225817.

[35] dos Santos Nascimento IJ, da Silva Rodrigues ÉE, da Silva MF, de Araújo-Júnior JX, de Moura RO. Advances in Computational Methods to Discover New NS2B-NS3 Inhibitors Useful Against Dengue and Zika Viruses. Curr Top Med Chem 2022;22. https://doi.org/10.2174/1568026623666221122121330.

[36] dos Santos Nascimento IJ, de Aquino TM, da Silva Júnior EF. Computer-Aided Drug Design of Anti-inflammatory Agents Targeting Microsomal Prostaglandin E 2 Synthase-1 (mPGES-1). Curr Med Chem 2022;29. https://doi.org/10.2174/0929867329666220317122948.

[37] Yu W, MacKerell Jr AD. Computer-Aided Drug Design Methods. Methods Mol Biol 1520 2017:85–106. https://doi.org/10.1007/978-1-4939-6634-9_5.

[38] Zoete V, Grosdidier A, Michielin O. Docking, virtual high throughput screening and in silico fragment-based drug design. J Cell Mol Med 2009;13:238–48. https://doi.org/10.1111/j.1582-4934.2008.00665.x.

[39] Yang SY. Pharmacophore modeling and applications in drug discovery: challenges and recent advances. Drug Discov Today 2010;15:444–50. https://doi.org/10.1016/j.drudis.2010.03.013.

[40] Lu X, Yang H, Chen Y, Li Q, He SY, et al. The Development of Pharmacophore Modeling: Generation and Recent Applications in Drug Discovery. Curr Pharm Des 2018;24:3424–39. https://doi.org/10.2174/1381612824666180810162944.

[41] Pirhadi S, Shiri F, Ghasemi JB. Methods and applications of structure based pharmacophores in drug discovery. Curr Top Med Chem 2013;13:1036–47. https://doi.org/10.2174/1568026611313090006.

[42] Tung MC, Fung KM, Hsu HM, Tseng TS. Discovery of 8-prenylnaringenin from hop (Humulus lupulus L.) as a potent monoacylglycerol lipase inhibitor for treatments of neuroinflammation and Alzheimer's disease. RSC Adv 2021;11:31062–72. https://doi.org/10.1039/d1ra05311f.

[43] Tsai KC, Zhang YX, Kao HY, Fung KM, Tseng TS. Pharmacophore-driven identification of human glutaminyl cyclase inhibitors from foods, plants and herbs unveils the bioactive property and potential of Azaleatin in the treatment of Alzheimer's disease. Food Funct 2022;13:12632–47. https://doi.org/10.1039/d2fo02507h.

[44] Tung MC, Tsai KC, Fung KM, Don MJ, Tseng TS. Characterizing the structure-activity relationships of natural products, tanshinones, reveals their mode of action in inhibiting spleen tyrosine kinase. RSC Adv 2021;11:2453–61. https://doi.org/10.1039/d0ra08769f.

[45] Tseng TS, Chuang SM, Hsiao NW, Chen YW, Lee YC, et al. Discovery of a potent cyclooxygenase-2 inhibitor, S4, through docking-based pharmacophore screening, in vivo and in vitro estimations. Mol Biosyst 2016;12:2541–51. https://doi.org/10.1039/c6mb00229c.

[46] Tung MC, Fung KM, Hsu HM, Tseng TS. Discovery of 8-prenylnaringenin from hop (Humulus lupulus L.) as a potent monoacylglycerol lipase inhibitor for treatments of neuroinflammation and Alzheimer's disease. RSC Adv 2021;11:31062–72. https://doi.org/10.1039/d1ra05311f.

[47] Khedkar SA, Malde AK, Coutinho EC, Srivastava S. Pharmacophore modeling in drug discovery and development: an overview. Med Chem 2007;3:187–97. https://doi.org/10.2174/157340607780059521.

[48] Guner OF. The impact of pharmacophore modeling in drug design. IDrugs 2005;8:567–72.

[49] Gao Q, Yang L, Zhu Y. Pharmacophore based drug design approach as a practical process in drug discovery. Curr Comput Aided Drug Des 2010;6:37–49. https://doi.org/10.2174/157340910790980151.

[50] Friedland N, Mack TR, Yu M, Hung LW, Terwilliger TC, et al. Domain orientation in the inactive response regulator Mycobacterium tuberculosis MtrA provides a barrier to activation. Biochemistry 2007;46:6733–43. https://doi.org/10.1021/bi602546q.

[51] He X, Wang L, Wang S. Structural basis of DNA sequence recognition by the response regulator PhoP in Mycobacterium tuberculosis. Sci Rep 2016;6:24442. https://doi.org/10.1038/srep24442.

[52] Li Y, Zeng J, Zhang H, He ZG. The characterization of conserved binding motifs and potential target genes for M. tuberculosis MtrAB reveals a link between the two-

component system and the drug resistance of M. smegmatis. BMC Microbiol 2010; 10:242. https://doi.org/10.1186/1471-2180-10-242.
[53] Genheden S, Ryde U. The MM/PBSA and MM/GBSA methods to estimate ligand-binding affinities. Expert Opin Drug Discov 2015;10. https://doi.org/10.1517/17460441.2015.1032936.
[54] Rastelli G, Del Rio A, Degliesposti G, Sgobba M. Fast and accurate predictions of binding free energies using MM-PBSA and MM-GBSA. J Comput Chem 2010;31. https://doi.org/10.1002/jcc.21372.
[55] Gogoi N, Chowdhury P, Goswami AK, Das A, Chetia D, et al. Computational guided identification of a citrus flavonoid as potential inhibitor of SARS-CoV-2 main protease. Mol Divers 2021;25. https://doi.org/10.1007/s11030-020-10150-x.
[56] Coban AY, Birinci A, Ekinci B, Durupinar B. Drug susceptibility testing of Mycobacterium tuberculosis by the broth microdilution method with 7H9 broth. Mem Inst Oswaldo Cruz 2004;99. https://doi.org/10.1590/S0074-02762004000100020.
[57] Uddin TM, Chakraborty AJ, Khusro A, Zidan BRM, Mitra S, et al. Antibiotic resistance in microbes: History, mechanisms, therapeutic strategies and future prospects. J Infect Public Health 2021;14:1750–66. https://doi.org/10.1016/j.jiph.2021.10.020.
[58] Seung KJ, Keshavjee S, Rich ML. Multidrug-Resistant Tuberculosis and Extensively Drug-Resistant Tuberculosis. Cold Spring Harb Perspect Med 2015;5:a017863. https://doi.org/10.1101/cshperspect.a017863.
[59] Dheda K, Gumbo T, Gandhi NR, Murray M, Theron G, et al. Global control of tuberculosis: from extensively drug-resistant to untreatable tuberculosis. Lancet Respir Med 2014;2:321–38. https://doi.org/10.1016/S2213-2600(14)70031-1.
[60] Allue-Guardia A, Garcia JI, Torrelles JB. Evolution of Drug-Resistant Mycobacterium tuberculosis Strains and Their Adaptation to the Human Lung Environment. Front Microbiol 2021;12:612675. https://doi.org/10.3389/fmicb.2021.612675.
[61] Matsushita M, Janda KD. Histidine kinases as targets for new antimicrobial agents. Bioorg Med Chem 2002;10:855–67.
[62] Barrett JF, Goldschmidt RM, Lawrence LE, Foleno B, Chen R, et al. Antibacterial agents that inhibit two-component signal transduction systems. Proc Natl Acad Sci USA 1998;95:5317–22.
[63] Worthington RJ, Blackledge MS, Melander C. Small-molecule inhibition of bacterial two-component systems to combat antibiotic resistance and virulence. Future Med Chem 2013;5:1265–84. https://doi.org/10.4155/fmc.13.58.
[64] Stephenson K, Hoch JA. Virulence- and antibiotic resistance-associated two-component signal transduction systems of Gram-positive pathogenic bacteria as targets for antimicrobial therapy. Pharm Ther 2002;93:293–305.
[65] Michio Kurosu EB. Bacterial protein kinase inhibitors. Drug Dev Res 2010;71:168–87.
[66] Stephenson K, Yamaguchi Y, Hoch JA. The mechanism of action of inhibitors of bacterial two-component signal transduction systems. J Biol Chem 2000;275:38900–4. https://doi.org/10.1074/jbc.M006633200.
[67] Garcia-Calderon CB, Casadesus J, Ramos-Morales F. Rcs and PhoPQ regulatory overlap in the control of Salmonella enterica virulence. J Bacteriol 2007;189:6635–44. https://doi.org/10.1128/JB.00640-07.
[68] Kundu M. The role of two-component systems in the physiology of Mycobacterium tuberculosis. IUBMB Life 2018;70:710–7. https://doi.org/10.1002/iub.1872.
[69] Ewann F, Jackson M, Pethe K, Cooper A, Mielcarek N, et al. Transient requirement of the PrrA-PrrB two-component system for early intracellular multiplication of Mycobacterium tuberculosis. Infect Immun 2002;70:2256–63. https://doi.org/10.1128/IAI.70.5.2256-2263.2002.
[70] Giordano D, Biancaniello C, Argenio MA, Facchiano A. Drug Design by Pharmacophore and Virtual Screening Approach. Pharm (Basel) 2022;15. https://doi.org/10.3390/ph15050646.